Normalized Steepness Index along the Himalayan Arc as a proxy for Indian plate segmentation

Raj Sunil Kandregula, Pavankumar, G*., Manglik, A.

CSIR-National Geophysical Research Institute, Uppal Road, Hyderabad – 500 007, INDIA

Corresponding Author:

Dr. G. Pavankumar
Room Nr. 113, Main Building
CSIR-National Geophysical Research Institute
Uppal Road, Hyderabad – 500007, INDIA.

Tel. : +91-40-27012884
Fax. : +91-40-23434651
Email : gayatripavan@ngri.res.in
Pavan.ngri@gmail.com

Abstract

The Indian plate underthrusting the Himalaya is considered to be segmented along the collision belt arc and seismic images of the Indian mantle lithosphere (IML) suggest along-arc variations in the angle of underthrusting and its northern limit beneath Tibet. The pre-existing transverse tectonic structures of the Indian plate mapped in the Ganga foreland basin have been related to these segmentation boundaries. These segmentations imply changes in mechanical properties of adjoining blocks which should manifest in the form of spatial variations in topography build-up. We have analysed a geomorphic index, normalized channel steepness (k_{sn}), along the Himalayan arc using the ALOS elevation dataset to test whether there is any correlation between the k_{sn} and these segmentation boundaries. Our results bring out spatial variability in the k_{sn} along the arc. Based on these results, the arc can be segmented into five blocks, similar to the ones delineated based on correlation between the width of the Ganga foreland basin and the disposition of major Himalayan thrusts from the foothills. Thus, the k_{sn} can be used as a proxy to demarcate different tectonic blocks along the Himalayan arc. Further, we have found a good correlation between the basin width and the northern limit of the IML for all block except the Uttarakhand block. We infer that transverse crustal heterogeneities in this block due to the continuation of different litho-units of the Aravalli-Delhi Fold Belt could be a plausible cause for this anti-correlation.

1. Introduction

Collision of the Indian plate with the Eurasian plate around ~55 Ma resulted in the formation of the ~2500 km long Himalayan mountain belt and the highest-altitude Tibetan Plateau on earth (Molnar and Tapponnier, 1975, Patriat and Achache, 1984). This vital process which shortens the lateral spreading of the Indian lithosphere, has been ongoing since then (Bilham et al., 1998; Avouac, 2003) and it is also conspicuous from the convergence along the Himalayan arc, Tibetan plateau due to the eastward rise of the earth's crust and southward transposition at the eastern syntaxes (Molnar and Lyon Caen, 1989; Wang et al., 2001; Zhang et al., 2004). This convergence is somewhat captivated by the shortening of the underthrusting Indian plate below the Tibetan plate and also consumed part of it by the Tibetan Plateau (Li and Song, 2018; Parsons et al., 2020). The inter-continental convergence between India and Eurasia has led to the generation of several strain zones, thrusts, highly fractured and jointed rock formations in the Himalayan terrain which caused instability due to seismic activity. Recent studies on the Himalayan deformation suggest that the southern Tibet has advanced towards India by sliding over the top of the underthrusting

Indian plate at a rate of ~16-18 mm/yr (Ghavri and Jade, 2021; Dal Zilio et al., 2020). This has resulted in piling up of the slip deficit and stresses at the northern stretch of the MHT which is currently locked to the Indian plate by friction at its base. About 10-20 mm/yr of varying shortening rates is suggested for the Himalayan arc from Nanga Parbat (west) to Namcha Burwa (east) (Jade et al., 2004).

The enduring convergence between the two tectonic plates generated several devastating earthquakes in the entire Himalayan arc since historical past making this region as one of the most seismically active regions of the world. The Himalayan orogenic belt has been struck by several devastating earthquakes in the past (Figure 1) viz., 1897 Shillong (Mw > 8), 1905 Kangra (Mw 7.8), 1934 Bihar-Nepal (Mw > 8), 1950 Tibet-Assam (Mw 8.6), 2005 Kashmir (Mw 7.6), 2015 Gorkha (Nepal, Mw 7.8) (Rajendran and Rajendran, 2005; Bilham, 2019). A number of geophysical investigations have been conducted across the Himalayan mountain belt to image the geometry of the MHT and its variations in different tectonic domains/segments of the collision zone and lithospheric structure that enhances the understanding of the ongoing orogenic evolution and earthquake genesis (Lyon-Caen and Molnar, 1985; Brown et al., 1996; Nelson and Zhao et al., 1996; Zhao et al., 1993; Hauck et al., 1998; Tiwari et al. 2006; Wittlinger et al., 2009; Nábělek et al., 2009; Acton et al., 2011; Nelson et al., 1996; Brown et al., 1996; Caldwell et al., 2013; Mahesh et al., 2013, Pavankumar et al., 2014, Pavankumar and Manglik, 2021).

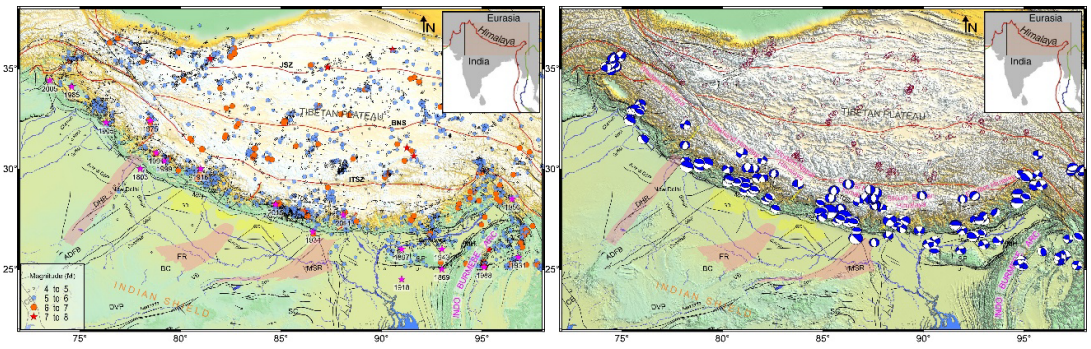

Figure 1. (a) Map showing seismicity distribution along the Himalayan arc (Source: European-Mediterranean Seismological Centre (EMSC) catalogue:1970-2022) and (b) focal mechanism of some of the earthquakes along the mountain belt. The fault plane solutions are taken from https://www.globalcmt.org/CMTsearch.html. The abbreviations are: ADFB – Aravalli Delhi fold belt; DVP – Deccan Volcanic Province; VB – Vindhyan Basin; BC – Bundelkhand craton; SC – Singhbhum craton; CB- Cambay basin; SP – Shillong Plateau; MH – Mikir Hills; DHR – Delhi - Haridwar Ridge; DSR – Delhi - Sargodha Ridge; FR – Faizabad Ridge; MSR – Monghyr - Saharsa Ridge; KCR – Kaurik-Chango rift; TR – Thankola rift; YR – Yadong rift; GD – Gandak depression; SD – Sharda depression; MFT – Main Frontal Thrust; MBT – Main Boundary Thrust; MCT – Main Central Thrust; STDS – South Tibetan Detachment System; ITSZ – Indus-Tsangpo Suture Zone; BNSZ – Bangong

Nujiang Suture Zone; LSSZ – Longmu Tso Shuanghu Suture Zone; JSSZ – Jinsha Suture Zone; AKSZ – Anyemaqen Kunlun Suture Zone; DF – Dauki fault.

Recent geophysical studies of the collision zone provided evidences of along arc variations in the Indian lithosphere that has been underthrusting beneath the Tibetan plateau, in terms of its dip (angle of underthrusting), northern extent of the Indian Mantle Lithosphere underneath the Tibetan Plateau, lateral variations of the MHT and subduction geometry through lateral discontinuities in the seismic velocities (Li et al., 2008; Zhao et al., 2010; Li and Song, 2018), analyses of gravity and elastic properties (Chen et al., 2015; Ravi Kumar et al., 2020) and by lateral changes in various physical parameters (e.g. Yin, 2006; Robert et al., 2011). Identifying these segment boundaries is of paramount significance in seismically active terrains, as these boundaries can confine the dimensions of faulting in a single earthquake to part of a fraction of the total length of fault, thereby restricting the size of the earthquake.

Segmentation identification studies along the Himalayan arc have been carried out in various disciplines. Seismological, GPS measurements and correlation between topography and Bouguer gravity anomaly provided insights for along-arc variations in the crustal-scale heterogeneities, displacement of the Main Himalayan Thrust (MHT), subducting plate angle and northward proliferation of the Indian lithosphere into the Himalayan-Tibetan system (Manglik et al. 2021; Dal Zilio et al. 2020; Bai et al. 2019; Li and Song, 2018; Singer et al., 2017; Elliott et al. 2016; Zhao et al. 2010). Shaokun et al. (2019) using the P-S wave velocities ratio advised diverse geometries from west to east for the underthrusting IML. Further, they contemplated that the slab tear up beneath the eastern Tibet and the delamination of lithosphere in the western Tibet are the two important factors that can explain the high Vp/Vs in the western and decreased Vp/Vs in the eastern segment of the Tibetan plateau. Robert et al. (2011) conducted thermochronological studies in the western and eastern parts of the central Nepal Himalaya and correlated the results with the data of eastern Nepal and Bhutan Himalaya which highlights the presence of lateral variations in the geometry of the MHT. They opined that there is no presence of crustal scale MHT ramp in the western Bhutan and there is a larger dip angle of mid-crustal ramp of the MHT in the central Nepal rather than in western Nepal

Kosarev et al. (1999) highlighted that the Indian lithosphere plunges towards north close to the Indus-Tsangpo (or Indus-Yarlung) suture and also it is separated from the surface under the central Tibet. Contrary to this, Tilmann et al. (2003) that the Indian plate underthrust the Tibetan plateau up to Bangong-Nujiang Suture (BNS), after that it might sink nearly vertical to at least 400 km depth. Liang et al. (2007) suggested a new tear model in which the Indian lithosphere is divided into two slabs, a north advancing slab subducting with

a steeper angle under the western part and a north-east advancing slab subducting at a shallower angle under the eastern sector of the Tibetan plateau. Additionally, they suggested that these two slabs are teared apart along the Yadong-Anduo-Golmund (YAG) tectonic corridor. Li et al. (2008) suggested that the P-wave travel time tomography unveils compelling lateral changes in the velocities and estimated the horizontal distance beyond which the inferred Indian lithosphere drifts northward under the plateau. They proposed that the IML decreases from west to east. Liang et al. (2012) come up with a new model suggesting that the segmented Indian slab while underthrusting in the south-central region of the Tibetan region with compelling lateral physical and compositional variations within the continental lithosphere.

Zhao et al. (2010) observed low-angle subduction of the Indian lithosphere in western Tibet on the basis of seismic discontinuities and suggested that the subduction angle gradually becomes steeper towards east. Li and Song (2018) used P and S wave seismic tomograms and advised that the Indian lithosphere is severed into four major segments with three main tears along the Himalayan arc with shallow dip angle of subduction towards east and west compared to the centre. Contrary to this, Dal Zilio et al. (2021) suggested that the western and eastern blocks have much steeper angles of subduction compared to the central block by analysing GPS measurements. Hetényi et al. (2016) examined the along-arc variations using the analysis of arc parallel topography and bouguer gravity anomaly data and suggested that the three major basement ridges i.e. DHR, FR and MSR played an important role in the segmentation of the Himalaya into four parts. They further implied that there is no correlation among the two factors that are considered. Ravi Kumar et al. (2020) analysed gravity, geoid and elevation data and inferred eastward decrease in the effective elastic thickness of the Indian lithosphere (58 km in west to the 36 km in east). Mandal et al. (2015) analysed the long-wavelength topography of the Himalayan hinterland and suggested the correlation of the varying topography with the along-arc variations in the underthrusting rate of the Indian plate.

Majority of these studies are confined only to the Himalaya-Tibetan region; however, the formation of the Himalayan Foreland basin and its geometry is also connected with the dynamics of the underthrusting Indian lithosphere and its pre-orogenic heterogeneities. Recently, Manglik et al. (2021) tested correlation between the foreland basin width and the disposition of major thrust faults (distance between MCT and MFT) by using several topographic and Bouguer gravity anomaly swath profiles crossing the Himalayan arc. The study inferred a new segmentation boundary which is possibly the extension of the Great Boundary Fault (GBF) towards north in the vicinity of the Indo-Nepal border separating Kumaun Himalaya from western Nepal Himalaya.

The fundamental objective of tectonic geomorphology is quantitative derivation of tectonic and geomorphic indicators from topography. Earth surface process models forecast landscape feedback to tectonic forcing whereby topography, erosion rates, and sediment production transiently alter to variations in tectonic boundary circumstances (Beaumont et al., 1992; Howard et al., 1994; Koons, 1989; Whipple & Tucker, 1999). Analysis of the steepness of the mountain belt can provide qualitative information on nature of the subsurface and fault segmentation (Kirby and Whipple, 2012). The normalized steepness index (k_{sn}) is proved to be useful in identifying large scale tectonic deformations (Wobus et al., 2006). As the topographic variations within the active margins can be linked to differential uplift of the rocks in the region, in the present study we have calculated the k_{sn} for the Himalaya and analysed the along arc variations of the k_{sn} and integrated the available structural variations of the Indian Mantle Lithosphere (IML) to identify possible correlation and to understand the related segmentation.

2. Method and Material:

2.1 Stream power incision model (SPIM): derivation of normalized steepness index

The Stream Power Incision Model (SPIM) is the most prevalent and frequently used technique to model the dynamics of bedrock channel systems (Howard, 1998). The incision rate (E) of the river bedrock channel can be represented by the product of erodibility of the bed rock (K), drainage area upstream to the river (A) and the topographic slope (S) along the river (Howard and Kirby, 1983; Lague, 2013) which is expressed as

$$E = K A^m S^n \quad (1)$$

where m and n are positive constants which are associated with basin lithology, hydraulic geometry and the erosion process (Snyder et al., 2000; Whipple and Tucker, 2002).

The detachment-limited mass balance equation affirms that the first order derivative of channel elevation (h) in relation to time (t) hinges on the rock uplift rate (U) and incision rate (E) (Royden and Perron, 2012; Han et al., 2017) that can be denoted as:

$$dh/dt = U\text{-}E \quad (2)$$

$$= U - K A^m S^n \quad (3)$$

or

$$dh/dt = U(X,t) - K(X,t)\, A(X,t)^m\, (dh/dX)^n \quad (4)$$

In equilibrium state, the rate of rock uplift is equal to channel incision, i.e.

$$dh/dt = (U/K)^{1/n} A(X)^{m/n} \quad (5)$$

Rearranging the above eq. and solving the equation for S under equilibrium conditions gives

$$S = (U/K)^{1/n} A(X)^{m/n} \quad (6)$$

The local channel slope can also be defined by replacing *(U/K)* with channel steepness (k_s) and m/n with θ (concavity index) which is expressed as

$$S = k_s A^{-\theta} \quad (7)$$

In general, the estimation of the concavity index (θ) and steepness index (k_s) can be obtained from the linear regression of gradient against drainage area on a log-log plot (Kirby and Whipple, 2012). However, little variations or uncertainties in the θ (regression slope) may cause large variations in the steepness index (regression intercept), hence, a normalized steepness index (k_{sn}) is needed to account for this autocorrelation. Thus, k_{sn} is evaluated by slope-area regression using a reference concavity index (θ_{ref}), where the θ_{ref} of the steady state channels falls in a restricted range of $0.4 \leq \theta \leq 0.6$. This permits efficient correlation of profiles of streams with significantly changing drainage area (Wobus et al. 2006).

We analysed all the major streams/rivers which cut across all the major thrust faults along the 2500 km long Himalayan orogenic belt for the calculation of k_{sn}. We used Advanced Land Observing Satellite (ALOS) World 3D (AW3D) Digital Elevation Model (DEM) (https://www.eorc.jaxa.jp/ALOS/en/aw3d30/index.htm) of 30m spatial resolution to extract the river drainage patterns. The AW3D 30m DEM is very effective especially in mountainous regions with high slopes and relief (Boulton and Stokes, 2018). Further, the drainage pattern extracted from this DEM is better in terms of resolution and very closely correlates with the original drainage pattern compared to the most commonly used DEM's, viz., SRTM and ASTER (Boulton and Stokes, 2018). The calculation of k_{sn} was carried out using the topo-toolbox in MATLAB, where the code was adopted from Schwanghart and Kuhn (2010) and Schwanghart and Scherler (2014).

The raw k_{sn} data obtained were interpolated using the kriging method and the interpolated data were then subjected to low-pass Gaussian filter of 5 passes. The resultant k_{sn} contours are then superimposed on an ALOS AW3D 30m spatial resolution DEM of the Himalayan

region (Figure 2). We have superimposed the boundaries of the inferred teared blocks of the IML and estimates of northern extent of the IML given by various researchers. The locations of the significant earthquakes that occurred in the region are also plotted.

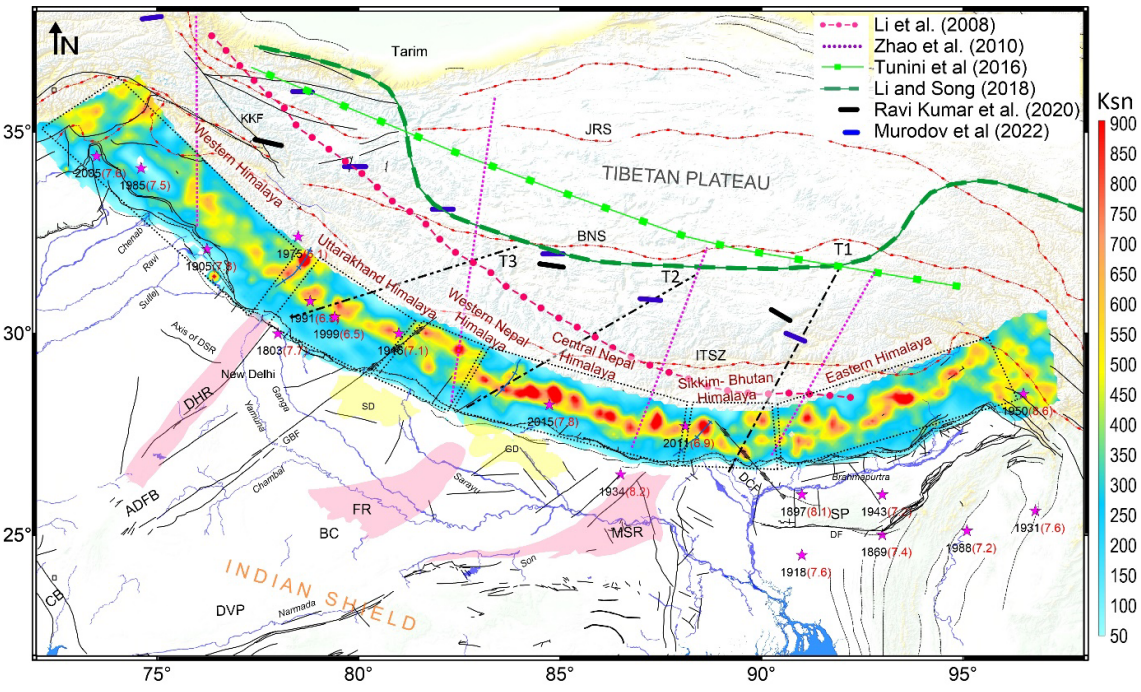

Figure 2. Map showing normalized river steepness index (k_{sn}) along the Himalayan arc. The northern boundary of the Indian plate proposed by Li et al. (2008), Zhao et al. (2010), Tunini et al. (2016), Li and Song (2018), Ravi Kumar et al. (2020) and Murodov et al. (2022) are also shown in the figure. Tearing of the Indian lithosphere inferred by Li and Song (2018) is shown as dashed lines, T1, T2, T3. Stars indicate the locations of the significant earthquakes that occurred in the region. Major geological and structural features are taken from the shape files available at the BHUKOSH portal of Geological Survey of India (http://bhukosh.gsi.gov.in/Bhukosh/MapViewer.aspx). For abbreviations please refer Figure. 1.

3. Results and Discussion

Broadly, the k_{sn} value ranges between 100 to 1000 with a general eastward increase in its value (Figure 2). The central part of the Himalayan arc, i.e., the central and eastern Nepal Himalaya region is associated with high k_{sn} values. The middle portion of the eastern Himalaya is also associated with high k_{sn} values. The detailed discussion on longitudinal wise variations of the k_{sn} for various segments of the arc is presented below.

3.1 Western Himalaya (Kashmir and Himachal) (WH, 74 – 78^{0}E longitude)

Previously, the region experienced major earthquakes that include 1905 Kangra earthquake (M 8.0) and 1985 and 2005 Kashmir earthquakes. The k_{sn} values of the western Himalaya

(till 78^{0}E) are low in comparison to other parts of the collision belt (Figure 2). Here, we attempt to explain build-up of topography in terms of strength of the colliding plates. As mountain building in a collision belt is linked to flexing of the underthrusting plate and the topography load applied on it, it can be understood that a high strength lithospheric plate will bend less under a constant applied load, providing a wider area of the plate for horizontal movement of the overlying thrust sheets and, thus, less build-up of the steep topography (Dahlen, 1990). Conversely, low strength of the plate and large angle of underthrusting shall facilitate piling up of thrust sheets giving rise to high topography (Figure 3). Thus, low k_{sn} values in this region may be considered as an indication of high strength of the Indian plate and low angle of underthrusting plate. This is substantiated by the results showing increased northward limit of the Indian mantle lithosphere beneath the Tibetan plateau for this region (Li et al., 2008; Li and Song, 2010).

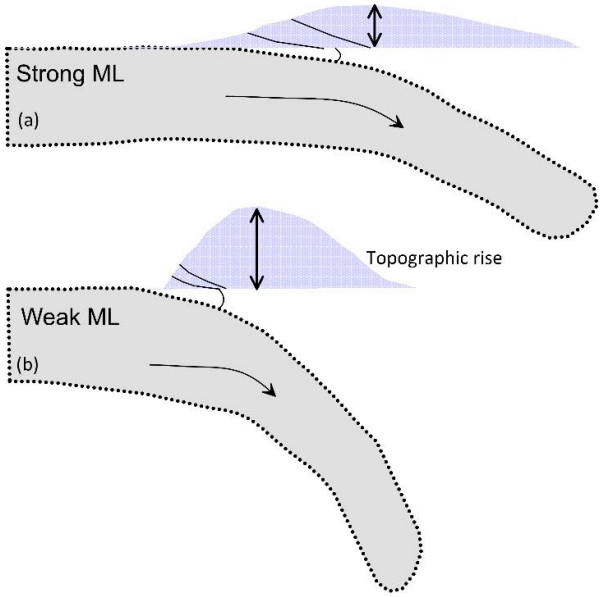

Figure 3. Schematic diagram showing relation between strength of the mantle lithosphere (ML) and topographic build-up

3.2 Uttarakhand Himalaya (UKH, 78-81^{o}E longitude)

This region experienced notable earthquake events that include 1991 Uttarkashi earthquake (M 6.7) and 1999 Chamoli earthquake (M 6.5). The entire Uttarakhand Himalaya is associated with moderate k_{sn} values with a couple of localized high k_{sn} zones (Figure 2). Interestingly, these anomalous high k_{sn} values are associated with the epicenters of the 1991 and 1999 earthquakes. The nature of k_{sn} pattern shows a NNE-SSW trend in the western part of the Uttarakhand Himalaya to the north of the MCT (Figure 2). We infer that this trend of the k_{sn} is an indication for extension of the DHR into the Higher Himalaya, which

is also supported by presence of rift-type morphology, (Kaurik-Chango rift) in the extreme north of the region (Arora et al., 2012) A recent seismological P-Receiver Function (P-RF) H-K stacking study (Mandal et al., 2021) has suggested the presence of three NS-to-NNE trending transverse structures beneath the Uttarakhand Himalaya characterized by significant Moho up-warp and large values (~1.85-2.13) of the ratio between the P- and the S-wave velocities. Manglik et al. (2022) suggested the extension of different litho-units of the Aravalli-Delhi Fold belt into the Delhi Seismic Zone and inferred their presence beneath the Uttarakhand Himalaya, leading to a spatially heterogeneous crust for this region. We therefore propose that the extension of DHR to the north of the MCT could represent the segment boundary that structurally divides the western Himalaya and the Uttarakhand Himalaya.

A study by Manglik et al. (2021) from the analysis of the basin width and the distance between the major thrusts (MFT and MCT) shows positive correlation in this part of the Himalaya. They considered this part of the Himalaya as one of the segments among the 5 major segments of the collision belt. They further opined that the Great Boundary Fault in the eastern side of the Uttarakhand Himalaya possibly separates this from western Nepal. A northward shift in the k_{sn} pattern supports the disposition of the major thrust faults in this segment (Figure 2). Moderate values of the k_{sn} suggest comparably strong IML with respect to western Himalaya, having low dip angle of the Indian plate, but high in comparison to the western Himalaya. We infer that in this segment of the Himalaya also, the IML extends to further north but not as much as it is in the western Himalaya. Zhao et al. (2010) have shown that the Indian plate subduction in this segment is getting steeper and reaches far north, almost to the Tarim Basin.

3.3 Western Nepal Himalaya (WNH, 81 - 83°E longitude)

We observe a lateral shift in the k_{sn} pattern (81.5-82.7°E) (Figure 2) which is correlating well with the previously inferred transverse faults of the western Nepal fault system (WNFS). Seismicity pattern is also well collaborating with this shift in the k_{sn} pattern where a cluster of earthquakes are concentrated in this zone (Figure 1). Faizabad ridge, one of the structurally important transverse ridges in the Ganga foreland basin, is located towards the eastern end of the region. Manglik et al. (2021) have shown negative and positive correlation in the basin width and relative displacement of MCT and MFT on either side, respectively, of the projection of the FR into the Himalaya and suggested a segment boundary in this region. However, magnetotelluric results of Demudu Babu et al. (2020) preclude northward

extension of the present inferred shape of the FR. They suggested that the FR, if present beneath the Himalaya, might have deviated from its present inferred position.

The k_{sn} values observed in this segment of the Himalaya is relatively high compared to the western and Uttarakhand Himalaya, which is mostly confined to northernmost region suggesting a weaker IML and steep angle of underthrusting for this region compared to that in the western Himalaya and Uttarakhand. Harvey et al. (2015) studied along-arc topographic discontinuities with the help of k_{sn} and seismicity distribution in the central Himalaya and proposed a tectonic boundary in this segment (82.5°E) with a steep (50°) ramp in the MHT beneath western Nepal. They also opined that the occurrence of recent tectonic activity in this zone is causing the rise in topography. Another study by Murphy et al. (2014) came up with the presence of western Nepal Fault System (WNFS) that likely serves as a demarcating boundary of the strain-segregated region of the WNH which contains a first-order structure in the 3D displacement field of the WNH range. Cannon and Murphy (2014) inferred that the seismotectonic model of the Central Nepal is not the same in the case of WNH as the formers model is relatively simple, whereas, the latter's model is complicated in terms of regional geology, micro-seismicity and other factors indicate evidence for structural duplexing underneath the lesser and higher Himalaya. However, contrary to this Subedi et al. (2018) inferred that the Moho in the WNH is mildly dipping north at about 40 km under the foothills to about 58 km below the Higher Himalaya and increase underneath the southern Tibet. They advised that the crustal structure of WNH is identical to that of the Central Nepal and Garhwal Himalaya of the Uttarakhand region.

Previous geophysical studies suggested that geometry of the MHT is laterally varying. Larson et al. (1999) and Van der Beek et al. (2002) suggested that the southern flat ramp of the MHT is relatively steep compared to that in the central Nepal. However, the dip of the mid-crustal MHT ramp is much steeper in central Nepal rather than the WNH (Berger et al., 2004). From the observed pattern of the k_{sn} and available geophysical data, we propose that the western Nepal Himalaya, lying west of the Faizabad ridge and east of the GBF, constitutes one of the segments of the Himalaya with relatively weak, relatively steeply dipping Indian lithosphere. One of the tearing boundaries of the Indian lithosphere proposed by Li and Song (2018) also coincides with this segment.

3.4 Central and Eastern Nepal Himalaya (83-88°E longitude)

The central Nepal Himalaya is characterized by high to very high k_{sn} values where this region experienced 1984 Bihar-Nepal earthquake (M 8.0) and very recent 2015 Gorkha earthquake (M 7.8). The location of the 2015 earthquake is associated with a zone of high

k_{sn} (Figure 2). There are several patches of high k_{sn} values observed in this zone which could be due to various transverse tectonic features existing in the region, e.g. Judi lineament, Gourishankar lineament (Mugnier et al., 2017). The high k_{sn} values observed in this zone suggest weaker part of the IML and steep dip angle of the Indian lithosphere. Manglik et al. (2021) has shown positive correlation of the basin width and relative separation of the major thrust sheets. Results from previous studies also support the less northward extent of the IML compared to that in the western Himalaya (Figure 2).

3.5 Sikkim and western Bhutan Himalaya (88-89°E longitude)

The k_{sn} pattern shows a prominent NNW-SSE trending linear high zone in this segment (Figure 2). This zone is prevailed by strike-slip deformation and deep crustal earthquakes on the planes oblique to the northward convergence of the Indian plate (Drukpa et al., 2006; Hazarika et al., 2010; Pavankumar et al., 2014; Paul and Mitra, 2015; Diehl et al., 2017; Pavankumar and Manglik, 2021). The Sikkim earthquake (Mw 6.9) of September 18, 2011 with the focal depth of 50 km (U.S Geological Survey (USGS); Ravi Kumar et al., 2012) is an example of such oblique deformation. Recent seismological and gravity studies carried out in the eastern segment of the Himalayan collision belt and adjoining foreland basin (Singer et al., 2017; Diehl et al., 2017; Grujic et al., 2018; Priestley, 2019) have recommended a NW-SE trending mid-crustal fault zone, termed as the Dhubri–Chungthang fault (DCF) extending from Chungthang locality in northeast Sikkim to Dhubri locality at the north-western edge of the Shillong Plateau that possibly breaks the Indian plate and the MHT underneath the eastern Himalaya. Pavankumar and Manglik (2021) using the broadband and long period magnetotelluric investigations suggested a NW-SE trending lithospheric-scale seismogenic fault that separates two geologically and compositionally distinct blocks of the Indian plate underthrusting the Himalaya beneath the MCTZ. It can be seen that the k_{sn} trend coincides with the NNW-SSE Dubri-Chunthang fault (DCF). Geophysical studies suggested that the structure of the underthrusting Indian lithosphere under the Sikkim Himalaya acts as a major factor responsible in dividing along-strike convergence across the Eastern Himalaya

A significant distinction in the structure of the Moho and the MHT in the Bhutan Himalaya has been ascertained from the receiver function analysis by Singer et al. (2017) which is also reflected in the k_{sn} patterns of the western and Eastern Bhutan. It is interesting to note that, although, the northern part of the western Himalaya is associated with the low to moderate k_{sn}, the Moho geometry shown by Singer et al. (2017) inferred an increased dip of the Moho south of the Higher Himalaya spreading almost 70 km depth, however, in eastern Bhutan the Moho is nearly sub-horizontal at 50 km depth. Contrary to this, Robert et al.

(2011) suggested the absence of crustal-scale MHT ramp in western Bhutan whereas increase in the dip of the mid-crustal ramp of the MHT in central Nepal. Previously, Hauck et al. (1998) inferred that westernmost Bhutan represents a changeover zone amidst the Bhutan and Nepal Himalaya which could be linked with the DCF. We therefore propose that the NW-SE trending DCF could be an active tectonic boundary that might separate the Sikkim and western Bhutan segment with the eastern Bhutan, similar to the GBF that possibly separates the Uttarakhand Himalaya with the western Nepal Himalaya.

3.6 Along arc-variations of the k_{sn} and its relation with the extent of IML

We attempted to see any qualitative relation between the k_{sn} pattern with the extent of Indian mantle lithosphere beneath the Tibetan plateau. We have plotted the northern extent of the Indian mantle lithosphere proposed by various researchers on Figure 2. Except Li and Song (2018), there is a gradual eastward decrease in the extent of the IML, suggesting the eastward decrease in the strength of the Indian lithosphere and increase in flexural bending beneath the Himalaya (Figure 2). This trend correlates well with the observed k_{sn} pattern. The Major tectonic/segmentation boundaries proposed from the present study, like DHR, GBF and DCF has good correlation with the Tears (T1, T2, T3), inferred from the velocity structure (Li and Song, 2018).

The logic behind varying geometries of the IML underneath the Tibet region might be associated with its intrinsic heterogeneity in its physical characteristics (Yin and Harrison, 2000) or may be due to the heterogeneities of the physical properties of the Asian Continental lithosphere along the collision zone (Chen et al., 2017). The heterogenous progression of the DHR, GBF, DCF etc., may have subjected the IML to tear near the already-existing feeble zones while its northward movement. This contrast between the moving slabs can be augmented by the positive correlation between the dip angle and the rollback velocity of the slab. This model is persistent with the previous works which inferred that the IML is underthrusting below the southern Tibet with a gradual increase in dip towards east (Chen et al., 2015; Li et al., 2008; Zhao et al., 2010). This is further supported by the most recent Pn tomography study (Li and Song, 2018), where a significant tearing is observed apparently at the same position.

From the results of the Pn tomography, the IML which was subjected to subduction is torn into pieces that are subducting at varying dip angles, in this due process, the northern limits of the IML became shallower, thereby extending further towards west and east with a gentle dip and getting steeper in the middle extending up to the BNS (Li and Song, 2018) (Figure 2). Ravi Kumar et al. (2020) from their 2D-density modelling results suggested that the Indian

lithosphere subducts laterally up to the Karakoram at a gentle angle in the west. In the central part, a high angle of subduction is observed up until the south of the BNS, while towards east it subducts at a shallow angle nearing the ITSZ and possibly further south of the BNS.

3.7 Width of the foreland basin and strength of the lithosphere

We tried to establish a possible relationship between the width of the foreland basin and the northern extent of the Indian plate along the arc using the profiles published by Manglik et al. (2021) (Figure 4). Lateral variations in the geometry of a foreland basin are linked to changes in the mechanical characteristics of the plate carrying load which is a consequence from the past tectonic events viz., rifting passive margin formation, as well as to changes in the loads introduced on it (Waschbusch and Royden, 1992; Millan et al., 1995). Since the estimated k_{sn} suggests lateral variations that infer the variations in the load imposed on the underthrusting Indian plate, we propose the variable nature of the geometry of the foreland basin also. As the structure of the foreland basin is controlled by the flexural rigidity which is controlled by strength of the Indian plate, we attempted to analyze any correlations in basin width and northern extent of the IML. We calculated the distance from the MFT to the IML proposed by Li et al. (2008) and plotted these values along with the distance between MFT and MCT against the distance between southern limit of the Indo-Gangetic Foreland basin to MFT as shown in Manglik et al. (2021). The relationship between these three parameters is shown in Figure 4. From the Figure 4, it can be seen that the width of the foreland basin and the northern extent of the IML is strongly correlated. Qualitative comparison between these two parameters also suggests segmentation of the Indian plate into different blocks. Major observation of our analysis is that for the Uttarakhand region, there is a negative correlation, which indeed infers along-strike segmentation of the foreland basin too (Figure 4). This segmentation might control the thickness and geometry of sedimentary sequences deposited in the foreland basin. Manglik et al. (2021, 2022) proposed the GBF of the Aravalli-Delhi Fold Belt as a major tectonic boundary segmenting the Indian plate between the Kumaun and the western Nepal sections of the Himalaya. It implies that the Indian plate underthrusting the Uttarakhand Himalaya should be more complex spatially than a simple horizontally layered crust-mantle architecture with bearing on the earthquake genesis for this segment of the Himalaya.

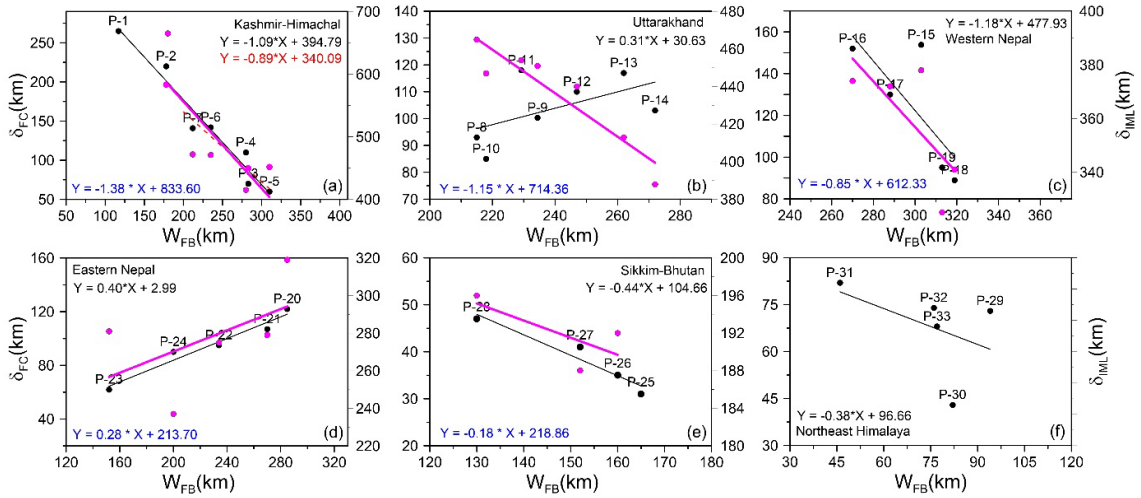

Figure 4. Relation between the width of the foreland basin (W_{FB}) and the extent of the Indian Mantle lithosphere (IML) from the Himalayan front (MFT) (δ_{IML}) [magenta colour line and dots] for the segments of the Himalayan arc proposed by Manglik et al. (2021). The black dots and lines are the relationship obtained by Manglik et al. (2021) between the W_{FB} and segment length between the MFT and MCT (δ_{FC}).

To analyse possible relationship between the k_{sn} and the Bouguer Gravity Anomalies (BGA), we have plotted the longitude-wise variations of k_{sn} and BGA along the MCT towards north with a swath of 10 km. The comparisons of these two parameters are shown in Figure 5. The trend of k_{sn} north of the MCT shows both positive and negative correlations. In sectors like western Himalaya and western Nepal, the trend shows good positive correlation whereas in parts of Uttarakhand and Sikkim-Bhutan segment it shows strong negative correlation (Figure 5). We infer that there is a relationship between k_{sn} and structural variations of individual segments. Manglik et al. (2021) have analysed 33 swath profiles of BGA cutting across the arc which displayed a significant along-arc variations as well as a change in its pattern across the foreland basin. They proposed that the lateral changes in the fabric of Indian plate could be responsible for these variations. Further, a cartoon depicting the segmentation boundaries are given in Figure 6.

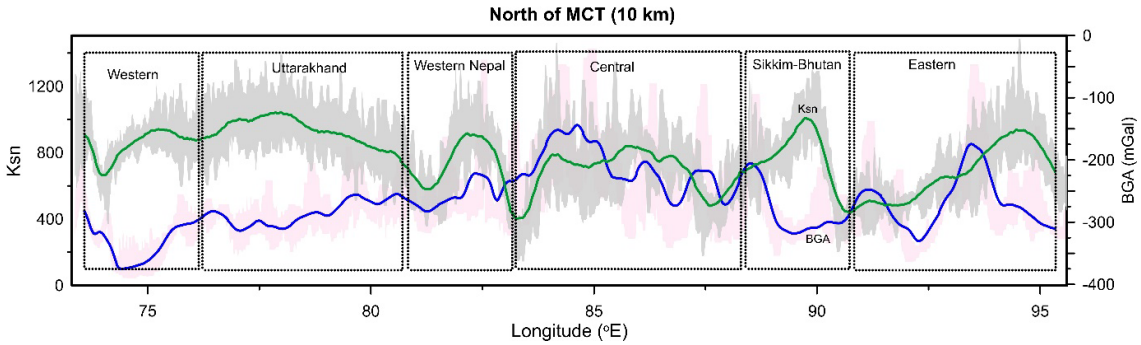

Figure 5: A comparison of longitudinal variations of the k_{sn} with the BGA. The red line indicates variations in k_{sn} and the blue line indicates variations in BGA. The profiles are taken with a swath width of 10 kms from the MCT.

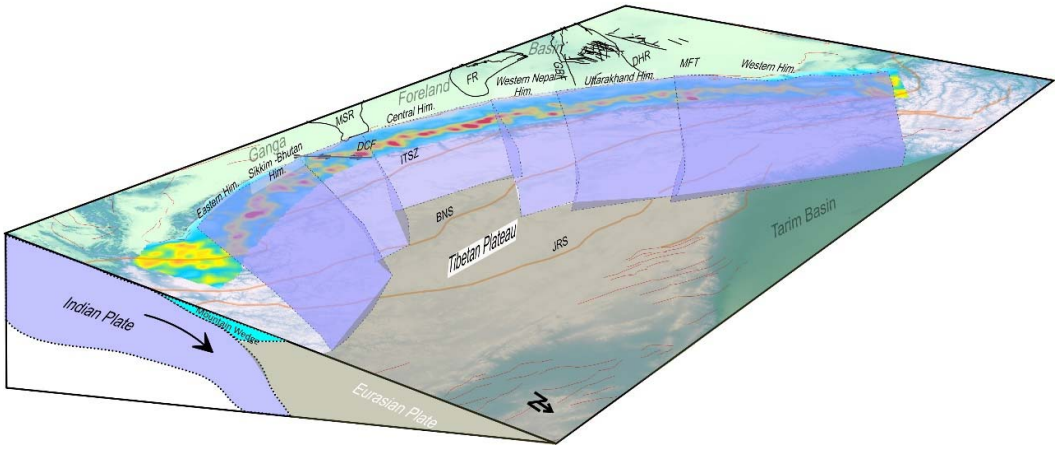

Figure 6: A Cartoon showing the segmented blocks of the Indian mantle lithosphere inferred from the present study.

4. Conclusions

Analysis of the normalized steepness Index computed for the Himalayan arc suggests prominent along-arc variations and has strong correlation with the strength of the Indian plate. By integrating the k_{sn} variations with the available geophysical information, we correlated the segmented nature of the underthrusting Indian plate with other studies and confirmed the presence of five major blocks. Various transverse tectonic features viz., the Delhi-Haridwar Ridge, the Great Boundary Fault, and the Dhubri-Chungthang Faults are inferred to be segmentaton boundaries. Hence, we conclude that the k_{sn} index can be used as a proxy to detect the segmentations in large scale tectonically active regions. A comparison of the foreland width with the northern limit of the Indian plate suggests segmented nature of the Ganga foreland basin with a significant variation in the Uttarakhand Himalaya. We propose the inherent structural heterogeneities within the Indian plate might be a possible reason for these segmentations. A detailed geophysical study to image three-dimensional lithospheric architecture of the plate including the Ganga foreland basin is necessary for better understanding of the geodynamic evolution of the Himalaya and robust estimates of the seismic potential of the collision belt.

Acknowledgements

The study has been carried out under the project MLP-FBR0003-28(AM) sponsored by Council of Scientific and Industrial Research (CSIR). KRS acknowledges the project for a post-doc fellowship. The work has been approved by CSIR-National Geophysical Research Institute (CSIR-NGRI) for publication as contribution number NGRI/Lib/2022/Pub-xxx under the project MLP6404-28(AM).

Data Availability Statement

The Digital Elevation Model data that was used in this study can be downloaded from the following link *https://www.eorc.jaxa.jp/ALOS/en/aw3d30/index.htm*.

References:

1. Acton, C., Priestley, K., Mitra, S. & Gaur, V. (2011). Crustal structure of the Darjeeling—Sikkim Himalaya and southern Tibet. *Geophys. J. Int. 184*, 829–852.
2. Arora, B.R., Gahalaut, V.K. and Naresh, K. (2012). Structural control on along-strike variation in the seismicity of the northwest Himalaya. Jour. Asian Earth Sci., v.57, pp.15–24.
3. Avouac, J. P. 2003. Mountain building, erosion and the seismic cycle in the Nepal Himalaya. Advances in Geophysics 46,1-80.
4. Demudu Babu, M., Manglik, A., Thiagarajan, S., Suresh, M. (2020). Electrical resistivity image of a basement ridge in the foreland central Ganga basin. *Journal of Applied Geophysics, 179*. https://doi.org/10.1016/j.jappgeo.2020.104097.
5. Bai L., Klemperer, S.L., Mori, J., Karplus, M.S., Ding, L., Liu, H., Li, G., Song, B. and Dhakal, S. (2019). Lateral variation of the Main Himalayan Thrust controls the rupture length of the 2015 Gorkha earthquake in Nepal. *Sci. Adv., 5*, eaav0723, doi: 10.1126/sciadv. aav0723.
6. Berger, A., Jouanne, F., Hassani, R. and Mugnier, J.L. (2004). Modelling the spatial distribution of present-day deformation in Nepal: how cylindrical is the Main Himalayan Thrust in Nepal?. *Geophysical Journal International, 156*: 94-114. https://doi.org/10.1111/j.1365-246X.2004.02038.x.
7. Berthet, T., Ritz, J.-F., Ferry, M., Pelgay, P., Cattin, R., Drukpa, D., Braucher, R., Hetényi, G. (2014). Active tectonics of the eastern Himalaya: New constraints from the first tectonic geomorphology study in southern Bhutan. *Geology, 42(5)*, 427–430.
8. Bilham, R. (2019). Himalayan earthquakes: a review of historical seismicity and early 21st century slip potential. *Geol. Soc. Lond. Spec. Publ. 483(1)*:423–482.
9. Bilham, R., Blume, F., Bendick, R. and Gaur, V. K. (1998). Geodetic constraints on the translation and deformation of India: implications for future great Himalayan earthquakes. *Current Science, 74*, 213-229.
10. Boulton, S.J. and Stokes, M. (2018). Which DEM is best for analyzing fluvial landscape development in mountainous terrains? *Geomorphology, 310*, pp.168–187.
11. Brown, L.D. Zhao, W., Nelson, K.D., Hauck, M., Alsdorf, D., Ross, A., Cogan, M., Clark, M., Liu, X., Che, J. (1996). Bright spots, structure, and magmatism in southern Tibet from INDEPTH seismic reflection profiling. *Science, 274*, 1688–1690.
12. Burov, E., and Diament, M. (1995). The effective elastic thickness (Te) of continental lithosphere: What does it really mean? *J. Geophys. Res., 100*, 3905– 3927.

13. Caldwell, W. B., Klemperer, S.L., Lawrence, S.F., Rai, S.S., Ashish. (2013). Characterizing the Main Himalayan Thrust in the Garhwal Himalaya, India with receiver function CCP stacking. *Earth and Planetary Science Letters,367*,15-27.

14. Cannon, J., & Murphy, M. (2014). Active lower crustal deformation and Himalayan seismic hazard revealed by stream channels and regional geology. *Tectonophysics, 633*. 10.1016/j.tecto.2014.06.031.

15. Chen, B., Liu, J., Chen, C., Du, J., & Sun, Y. (2015). Elastic thickness of the Himalayan-Tibetan orogen estimated from the fan wavelet coherence method, and its implications for lithospheric structure. *Earth and Planetary Science Letters, 409*, 1–14. https://doi.org/10.1016/j.epsl.2014.10.039.

16. Chen, M., Niu, F., Tromp, J., Lenardic, A., Lee, C. T. A., Cao, W., & Ribeiro, J. (2017). Lithospheric foundering and under thrusting imaged beneath Tibet. *Nature Communications, 8(1)*, 15659. https://doi.org/10.1038/ncomms15659.

17. Dahlen, F. A., (1990). Critical taper model of fold-and-thrust belts and accretionary wedges. *Annual Review of Earth and Planetary Science, 18*, 55–99, doi:10.1146/annurev.ea.18.050190.000415.

18. Dal Zilio, L., Hetényi, G., Hubbard, J. and Bollinger, L. (2021). Building the Himalaya from tectonic to earthquake scales. *Nat. Rev. Earth Environ., 2*, pp.251–268.

19. Dal Zilio, L., Jolivet, R., Van Dinther, Y. (2020). Segmentation of the Main Himalayan Thrust illuminated by Bayesian inference of interseismic coupling. *Geophys. Res. Lett. 47(4)*: e2019GL086424.

20. Diehl, T., Singer, J., Hetényi, G., Grujic, D., Clinton, J., Giardini, D., Kissling, E., Group, G.W. (2017). Seismotectonics of Bhutan: evidence for segmentation of the Eastern Himalayas and link to foreland deformation. *Earth Planet. Sci. Lett., 471*, pp. 54-64.

21. Drukpa, D., Velasco, A., Doser, D. (2006). Seismicity in the Kingdom of Bhutan (1937–2003): Evidence for crustal transcurrent deformation. *Journal of Geophysical Research, 111*. 10.1029/2004JB003087.

22. Elliott, J.R., Jolivet, R., González, P.J., Avouac, J., Hollingsworth, J. and Searle, M.P. (2016). Himalayan megathrust geometry and relation to topography revealed by the Gorkha earthquake. *Nature Geosci., 9*, pp.174–180.

23. Ghavri, S., Jade, S. (2021). Seismic potential of megathrust in the Kumaun-Garhwal region of NW Himalaya: implications from geodetic and seismic strain rates. *International Journal of Earth Sciences. 110*:1439–1452. https://doi.org/10.1007/s00531-021-02023-x.

24. Godin, L., La Roche, R.S., Waffle, L. and Harris, L.B. (2018). Influence of inherited Indian basement faults on the evolution of the Himalayan Orogen. *Geological Society, London, Special Publications*, *481*, pp. 251 – 276, https://doi.org/10.1144/SP481.4.

25. Grujic, D., Hetényi, G., Cattin, R., Baruah, S., Benoit, A., Drukpa, D., Saric, Adi. (2018). Stress transfer and connectivity between the Bhutan Himalaya and the Shillong Plateau. *Tectonophysics, 744*. 322-332. 10.1016/j.tecto.2018.07.018.

26. Hammer, P., Berthet, T., Hetényi, G., Cattin, R., Drukpa, D., Chophel, J., Lechmann, S., Moigne, N. Le, Champollion, C., and Doerflinger, E. (2013). Flexure of the India plate underneath the Bhutan Himalaya. *Geophys. Res. Lett., 40*, 4225- 4230. doi:10.1002/grl.50793.

27. Hammer, P., Berthet, T., Hetényi, G., Cattin, R., Drukpa, D., Chophel, J., Lechmann S., Le Moigne, N., Champollion, C., and Doerflinger, E. (2013). Flexure of the India plate underneath the Bhutan Himalaya. *Geophys. Res. Lett., 40* pp: 4225–4230, doi:10.1002/grl.50793.

28. Han, Z., Li, X., Wang, N., Chen, G., Wang, X., Lu, H. (2017). Application of river longitudinal profile morphometrics to reveal the uplift of Lushan Mountain. *Acta Geologica Sinica- English Edition, 91 (5)*, 1644–1652.

29. Harvey, J., Burbank, D., Bookhagen, B. (2015). Along-strike changes in Himalayan thrust geometry: Topographic and tectonic discontinuities in western Nepal. *Lithosphere, 7*. 10.1130/L444.1.

30. Hauck, M. L., Nelson, K. D., Brown, L. D., Zhao, W., Ross. A. R. (1998). Crustal structure of the Himalayan orogen at ~90° east longitude from Project INDEPTH deep seismic reflection profiles. *Tectonics, 17*, 481– 500, doi:10.1029/98TC01314.

31. Hazarika, P., Kumar, M., Gudhimella, S., Raju, P., Rao, N., Srinagesh, D. (2010). Transverse Tectonics in the Sikkim Himalaya: Evidence from Seismicity and Focal-Mechanism Data. *Bulletin of The Seismological Society of America, 100*. 1816-1822. 10.1785/0120090339.

32. Hetényi, G., Cattin, R., Berthet T., Le Moigne, N., Chophel, J., Lechmann, S., Hammer, P., Drukpa, D., Sapkota, S.N., Gautier, S. and Thinley, K. (2016). Segmentation of the Himalayas as revealed by arc-parallel gravity anomalies. *Sci. Rep., 6*, 33866.

33. Hetényi, G., Cattin, R., Vergne, J.,and Nábèlek, J.L., (2006). The effective elastic thickness of the India Plate from receiver function imaging, gravity anomalies and thermomechanical modelling, Geophys. *J. Int., 167,* pp: 1106–1118, doi:10.1111/j.1365-246X.2006.03198.x.

34. Howard, A.D. (1998). Long profile development of bedrock channels, Interaction of weathering, mass wasting, bed erosion, and sediment transport. *Geophysical Monograph American Geophysical Union*. *107*, 297–319.

35. Howard, A.D., Kirby, G. (1983). Channel changes in badlands. *Geol. Soc. Am. Bull. 94*, 739–752.

36. Jade, S. (2004). Estimates of plate velocity and crustal deformation in the Indian subcontinent using GPS geodesy. *Current Science, 86*, 1343-1348.

37. Jordan, T.A., and Watts, A.B. (2005). Gravity anomalies, flexure and the elastic thickness structure of the India–Eurasia collisional system. *Earth Planet. Sci. Lett., 236*, pp: 732–750.

38. Kirby, E., Whipple, K, X. (2012). Expression of active tectonics in erosional landscapes. *Journal of Structural Geology*, *44*, 54-75.

39. Kosarev, G., Kind, R., Sobolev, S.V., Yuan, X., Hanka, W., Oreshin, S. (1999). Seismic evidence for detached Indian lithospheric mantle beneath central Tibet. *Science, 283*, 1306–1308.

40. Lague, D. (2013). The stream power river incision model, evidence, theory and beyond. *Earth Surf. Process. Landforms 39 (1)*, 38–61.

41. Larson, K., Burgmann, R., Bilham, R., Freymuller, J. (1999). Kinematics of the India-Eurasia collision Zone from GPS measurements. *Journal of Geophysical Research: Solid Earth, 104.* 10.1029/1998JB900043.

42. Li, C., Hilst, R.D.V.D., Meltzer, A.S., Engdahl, E.R. (2008). Subduction of the Indian lithosphere beneath the Tibetan Plateau and Burma. *Earth Planet. Sci. Lett., 274*, pp. 157-168.

43. Li, J. and Song, X. (2018). Tearing of Indian mantle lithosphere from high-resolution seismic images and its implications for lithosphere coupling in southern Tibet. *Proc. Natl. Acad. Sci., 115*, pp.8296-8300.

44. Liang, X., & Sandvol, Eric & Chen, Youqiang & Hearn, Thomas & Ni, James & Klemperer, Simon & Shen, Yang & Tilmann, Frederik. (2012). A fragmented Indian slab and no south-verging subduction. *Earth and Planetary Science Letters, 333-334*. 101-111.

45. Liang, X., Shen, Y., Chen, J., Ren, Y. (2007). Crustal and mantle velocity models of southern Tibet from finite frequency tomography. *Journal of Geophysical Research: Solid Earth, 116,* 10.1029/2009JB007159.

628 46. Lyon-Caen, H. & Molnar, P. (1985). Constraints on the structure of the Himalaya from an
629 analysis of gravity anomalies and a flexural model of the lithosphere. *J. Geophys. Res. Solid*
630 *Earth, 88*, 8171–8191.

631 47. Mahesh, P., Rai, S., Sivaram, K., Paul, A., Gupta, S., Sarma, R., Gaur, V. (2013). One-
632 dimensional reference velocity model and precise locations of earthquake hypocenters in the
633 Kumaon-Garhwal Himalaya. *Bulletin of the Seismological Society of America, 103(1)*, 328–
634 339.

635 48. Mandal, N., Bose, S., Baruah, A., Sarkar, S. (2015). First-order topography of the Himalayan
636 Mountain belt: A deep-crustal flow analysis. *Geological Society, London, Special Publications*,
637 *412*. 10.1144/SP412.9.

638 49. Manglik, A., Kandregula, R.S., Gayatri, P.K. (2022). Foreland Basin Geometry and Disposition
639 of Major Thrust Faults as Proxies for Identification of Segmentation along the Himalayan Arc.
640 *Journal of the Geological Society of India, 98,* 57-61. https://doi.org/10.1007/s12594-022-1928-
641 y.

642 50. McNutt, M., Diament, M, Kogan, M. (1988). Variations of Elastic Plate Thickness at
643 Continental Thrust Belts. *Journal of Geophysical Research, 93*. 8825-8838.
644 10.1029/JB093iB08p08825.

645 51. Molnar, P. and Lyon Caen, H. (1989). Fault-plane solutions of earthquakes and active tectonics
646 of the Tibetan plateau and its margins. *Geophysical Journal International, 99*, 123–153.

647 52. Molnar, P. and Tapponnier, P. (1975). Cenozoic tectonics of Asia: effects of a continental
648 collision. *Science, 189*, 419-426.

649 53. Mugnier, Jean-Louis., Jouanne, F., Bhattarai, R., Cortés-Aranda, J., Gajurel, A., Leturmy, P.,
650 Robert, X., Upreti, B., Vassallo, R. (2017). Segmentation of the Himalayan megathrust around
651 the Gorkha earthquake (25 April 2015) in Nepal. *Journal of Asian Earth Sciences, 141*.
652 10.1016/j.jseaes.2017.01.015.

653 54. Murodov, D., Mi, W., Murodov, A., Oimuhmmadzoda, I., Abdulov S., Xin W. (2022). Deep
654 Crustal Structure Beneath the Pamir–Tibetan Plateau: Insights from the Moho Depth and Vp/Vs
655 Ratio Variation. *Frontiers in Earth Science*, 10.10.3389/feart.2022.821497.

656 55. Murphy, M., Taylor, M., Gosse, J., Silver, C., Whipp, D., Beaumont, C. (2014). Limit of strain
657 partitioning in the Himalaya marked by large earthquakes in western Nepal. *Nature Geoscience.*
658 *7, 38.* 10.1038/ngeo2017.

659 56. Nábělek, J., G. Hetényi, J. Vergne, S. Sapkota, B. Kafle, M. Jiang, H. Su, J. Chen, B. Huang,
660 and the Hi-CLIMB Team. (2009). Underplating in the Himalaya-Tibet collision zone revealed
661 by the Hi-CLIMB experiment. *Science, 325,* 1371–1374, doi:10.1126/science.1167719.

662 57. Nelson, K.D., Zhao, W., Brown, L.D., Kuo, J., Che, J. (1996). Partially molten middle crust
663 beneath southern Tibet: synthesis of project INDEPTH results. *Science, 274*, pp. 1684-1688,
664 10.1126/science.274.5293.1684.

665 58. Parsons, A. J., Hosseini, K., Palin, R. M., Sigloch, K. (2020). Geological, geophysical and plate
666 kinematic constraints for models of the India-Asia collision and the post-Triassic central Tethys
667 oceans. *Earth-Science Reviews, 208*, 103084. https://doi.org/10.1016/j.earscirev.2020.103084

668 59. Patriat, P. and Achache, J. (1984). India–Eurasia collision chronology has implications for
669 crustal shortening and driving mechanism of plates. *Nature, 311*, 615–621.

670 60. Paul, H., Mitra, S., Bhattacharya, S., Suresh, G. (2015). Active transverse faulting within
671 underthrust Indian crust beneath the Sikkim Himalaya. *Geophys. J. Int., 201*., pp. 1072-1083.

672 61. Pavankumar, G., Manglik, A., (2021). Complex tectonic setting and deep crustal seismicity of
673 the Sikkim Himalaya: An electrical resistivity perspective. *Physics and Chemistry of the Earth,*
674 *Parts A/B/C,124(2)*. https://doi.org/10.1016/j.pce.2021.103077.

675 62. Pavankumar, G., Manglik, A., Thiagarajan, S. (2014). Crustal geoelectric structure of the
676 Sikkim Himalaya and adjoining Gangetic foreland basin. *Tectonophysics, 637*, 238-250.
677 https://doi.org/10.1016/j.tecto.2014.10.009.

678 63. Priestley, K., Ho, T., and Mitra, S. (2019). The Crustal Structure of the Himalaya: A Synthesis.
679 *Geol. Soc. Lond. Spec. Publications 483*, 483–516. doi:10.1144/SP483-2018-127.

680 64. Rajendran, C.P., Rajendran, K. (2005). The status of central seismic gap: a perspective based on
681 the spatial and temporal aspects of the large Himalayan earthquakes. *Tectonophysics, 395*:19–
682 39.

683 65. Ravi Kumar, M., Hazarika, P., Prasad, G.S., Singh, A., Saha, S. (2012). Tectonic implications
684 of the September 2011 Sikkim earthquake and its aftershocks. *Curr Sci. 102*:788–792.

685 66. Ravi Kumar, M., Singh, B., Pavan Kumar, V., Satyakumar, A. V., Ramesh, D. S., & Tiwari, V.
686 M. (2020). Lithospheric density structure and effective elastic thickness beneath Himalaya and
687 Tibetan plateau: Inference from the integrated analysis of gravity, geoid, and topographic data
688 incorporating seismic constraints. *Tectonics, 39*, e2020TC006219.
689 https://doi.org/10.1029/2020TC006219

690 67. Robert, X., Van der Beek P., Braun J., Perry C., Mugnier J.L. (2011). Control of detachment
691 geometry on lateral variations in exhumation rates in the Himalaya: insights from low-
692 temperature thermochronology and numerical modelling. *J. geophys. Res., 116*, pg. B05202,
693 doi:10.1029/2010JB007893.

694 68. Royden, L, Perron, J.T. (2012). Solutions of the stream power equation and application to the
695 evolution of river longitudinal profiles. *Journal of Geophysical Research Earth Surf. 118 (2),*
696 497–518.

697 69. Schwanghart, W., Kuhn, N. J., (2010). TopoToolbox: A set of Matlab functions for topographic
698 analysis. *Environmental Modelling & Software 25(6)*, 770–781.

699 70. Schwanghart, W., Scherler, D. (2014). Short Communication: TopoToolbox 2 – MATLAB-
700 based software for topographic analysis and modelling in Earth surface sciences. *Earth Surface*
701 *Dynamics 2(1)*, 1–7.

702 71. Shaokun Si., Gao, R., Tian, X. (2019). Eastwest differential under thrusting of the Indian
703 lithospheric plate beneath central Tibet revealed by imaging VP/VS. *Journal of Geophysical*
704 *Research: Solid Earth, 124,* 9714–9730. https://doi.org/10.1029/2018JB017259

705 72. Singer, J., Kissling, E., Diehl, T., Hetényi, G. (2017). The under thrusting Indian crust and its
706 role in collision dynamics of the Eastern Himalaya in Bhutan: insights from receiver function
707 imaging. *J. Geophys. Res. Solid Earth*, 122, pp. 1152-1178.

708 73. Snyder, N.P., Whipple, K.X., Tucker, G.E., Merrittis, D.J. (2000). Landscape response to
709 tectonic forcing, Digital elevation model analysis of stream profiles in the Mendocino triple
710 junction region, northern California. *GSA Bulletin 112 (8),* 1250–1263.

711 74. Subedi, S., Hetényi, G., Vergne, J., Bollinger, L., Lyon-Caen, H., Farra, V. (2018). Imaging the
712 Moho and the Main Himalayan Thrust in Western Nepal with receiver functions. *Geophysical*
713 *Research Letters, 45*, 13,222– 13,230. https://doi.org/10.1029/2018GL080911.

714 75. Tilmann, F., Ni, J. (2003). Seismic Imaging of the Downwelling Indian Lithosphere Beneath
715 Central Tibet. *Science (New York, N.Y.). 300. 1424-7*. 10.1126/science.1082777.

716 76. Tiwari, V. M., Vyghreswara Rao, M. B. S., Mishra, D. C., Singh, B. (2006). Crustal structure
717 across Sikkim, NE Himalaya from new gravity and magnetic data. *Earth Planet. Sci. Lett., 247*,
718 61–69.

719 77. Tunini, L., Jiménez-Munt, I., Fernandez, M., Vergés, J., Villaseñor, A., Melchiorre, M., &
720 Afonso, J. C. (2016). Geophysical-petrological model of the crust and upper mantle in the
721 India-Eurasia collision zone. *Tectonics, 35*, 1642–1669. https://doi.org/10.1002/2016TC004161

78. Van der Beek, P., Champel, B., Mugnier, Jean-Louis. (2002). Controls on drainage development in regions of active fault-propagation folding. *Geology, 30*. 10.1130/0091-7613(2002)030<0471: CODDOD>2.0.CO;2.

79. Wang, Q., Zang, P., Freymueller, J. T., Bilham, R., Larson, K. M., Lai, X., You, X., Niu, Z., Wu, J., Li, Y., Yang, Z., and Chen, Q. (2001). Present day crustal deformation in China constrained by Global Positioning System measurements. *Science, 294*, 574-577.

80. Whipple, K.X., Tucker, G.E. (2002). Implications of sediment-flux-dependent river incision models for landscape evolution. *Journal of Geophysical Research Solid Earth. 107* (B2) ETG-3.

81. Wittlinger, G., Farra, V., Hetényi, G., Vergne, J., Nábělek, J. (2009). Seismic velocities in Southern Tibet lower crust: A receiver function approach for eclogite detection. *Geophys. J. Int., 177,* 1037–1049, doi:10.1111/j.1365-246X.2008.04084. x.

82. Wobus, C., Whipple, K.X., Kirby, E., Snyder, N., Johnson, J., Spyropolou, K., Crosby, B., Sheehan, D., Willett, S.D. (2006). Tectonics from topography, Procedures, promise, and pitfalls. *Spec. Pap. Geol. Soc. Am. 398*, 55.

83. Yin, A. (2006). Cenozoic tectonic evolution of the Himalayan orogen as constrained by along-strike variation of structural geometry exhumation history and foreland sedimentation. *Earth Sci. Rev., 71*:1–131.

84. Yin, A., Harrison, T. (2000). Geologic Evolution of the Himalayan-Tibetan Orogen. *Annual Review of Earth and Planetary Sciences, 28*. 211-280. 10.1146/annurev.earth.28.1.211.

85. Zhang, P., Shen, Z., Wang, M., Gan, W., Burgmann, R., Molnar, P., Wang, Q., Niu, Z., Sun, J., Wu, J., Hanrong, S. and Xinzhao, Y. (2004). Continuous deformation of the Tibetan Plateau from global positioning system data. *Geology, 32 (9)*, 809-812.

86. Zhao, J., Yuan, X., Liu, H., Kumar, P., Pei, S., Kind, R., Zhang, Z., Teng, J., Ding, L., Gao, X., Xu, Q. and Wang, W. (2010). The boundary between the Indian and Asian tectonic plates below Tibet. *Proc. Natl. Acad. Sci., 107*, pp.11,229–11,233.

87. Zhao, W. J., K. D. Nelson, and Project INDEPTH Team (1993). Deep seismic reflection evidence for continental under thrusting beneath southern Tibet. *Nature, 366*, 557–559.

X-X-X